ELSEVIER

S0032-3861(96)00296-0

Polymer Vol. 37 No. 20, pp. 4443–4453, 1996

0032-3861/96/$15.00 + 0.00

polymer papers

Blends of amorphous-crystalline block copolymers with amorphous homopolymers. Morphological studies by electron microscopy and small angle scattering

Kazuo Sakurai* and William J. MacKnight†
Polymer Science and Engineering Department, University of Massachusetts, Amherst, MA 01003, USA

and David J. Lohse, Donald N. Schulz and Joseph A. Sissano
Corporate Research Laboratories, Exxon Research & Engineering Company, Annandale, NJ 08801, USA

and Jar-Shyong Lin
Center for Small-Angle Scattering Research, Solid State Division, Oak Ridge National Laboratory, Oak Ridge, TN 37831, USA

and Mikhail Agamalyan
Brookhaven National Laboratory, Upton, NY 11973, USA
(Received 18 October 1995; revised 25 January 1996)

A morphological study was performed with symmetric diblock ethylene–propylene copolymer (DEP) and the binary blends made from DEP and atactic polypropylene (APP) by use of small angle X-ray, light and neutron scattering, and also scanning and transmission electron microscopy. DEP contains a crystallizable polyethylene block and an amorphous atactic polypropylene block. Quenching the blends in liquid nitrogen preserved the morphology in the melt state. This quenching technique revealed that DEP forms a lamellar microdomain structure and blending DEP and APP includes morphological changes in the microdomain structures as well as macrophase separation. When the APP chain was shorter than the APP block, the addition of APP changed the morphology from a lamellar to a bicontinuous cylindrical and then a discrete cylindrical and finally to a spherical structure. On the other hand, when the APP chain was longer than the APP block, macrophase separation was observed and only a transition from a lamella to a bicontinuous cylinder occurred. These morphological transitions in the melt state can be correlated to differences in the crystallization kinetics of the blends. Copyright © 1996 Elsevier Science Ltd.

(Keywords: blends; symmetric diblock copolymers; semicrystalline block)

INTRODUCTION

Block copolymers form various types of microdomain structures when the molecular weight is high enough to induce microphase separation[1–4]. A key parameter for determining the morphology is the ratio of the volume fraction (V_f) of the blocks. Lamellar structures are the thermodynamically most stable form if the volume fractions are nearly equal, and this is the case of the so-called symmetrical block copolymer. When the V_f of one block is greater than about 0.62, the morphology changes to bicontinuous forms (such as gyroic or double diamond), then cylindrical, and finally to spherical microstructures at still higher V_f. These structural transitions can also be induced by blending with homopolymers. Thomas and coworkers[2–4] studied blends of homo-polystyrene and poly(styrene-*b*-isoprene) or poly(styrene-*b*-butadiene) in a wide range of molecular weights and compositions. Winey *et al.*[2] summarized the morphological data and constructed a morphological diagram for this system which might be generally extended to blends of symmetrical diblock copolymers (d-AB) with their corresponding homopolymers (h-A). According to these authors, the morphology of the blends is determined by two parameters, the volume fraction and the relative homopolymer molecular weight ($M_{h\text{-}A}/M_{d\text{-}A}$), which is defined by dividing the molecular weight of h-A by that of A in d-AB. When $M_{h\text{-}A}/M_{d\text{-}A} > 1$, macrophase separation dominantly occurs. When $M_{h\text{-}A}/M_{d\text{-}A} < 1$, blending can induce morphological transitions.

In this series of work[5–7] we have explored the crystallization kinetics in the blends made from

* Permanent address: Research and Development Center, Kanebo Ltd., 1-5-90 Tomobuchi-cho, Miyakojima-ku, Osaka, Japan
† To whom correspondence should be addressed

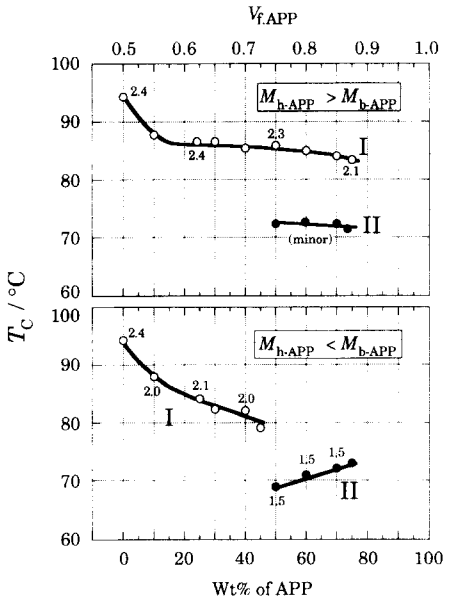

Figure 1 APP composition dependence of the crystallization temperature (T_c) for APP190 blends in the upper panel and APP15 blends in the lower one. T_c was determined as an onset temperature in d.s.c. cooling thermograms scanned at 10°C min^{-1} and classified into two types, I and II. The numbers attached to some data points indicate the Avrami exponent obtained in the isothermal crystallization[5]

symmetrical diblock ethylene–propylene copolymer (DEP) and atactic polypropylene (APP). Our data show that the crystallization behaviour of the polyethylene block (b-PE) is strongly related to both the molecular weight and composition of APP blended (see *Figure 1*). These phenomena can be interpreted on the assumption that addition of APP15 (see *Table 1*) induces morphological transitions in the b-PE microdomain in the melt state in a manner corresponding to the styrene/styrene-*b*-butadiene blend system[5]. However, although this is a reasonable assumption, it is nevertheless necessary to examine the morphology of the microdomains for DEP and APP blends directly in order to prove the point.

Pioneering work on the microdomain morphology of block copolymers and their blends was carried out by Thomas and coworkers[2–4] using transmission electron microscopy (TEM) and by Hashimoto and coworkers[9,10] using small angle X-ray scattering (SAXS) on the styrene–butadiene or styrene–isoprene systems. In the case of polyolefin blends, however, such techniques are not applicable because of the absence of sufficient electron density difference between microphases for SAXS and of chemical bonds which can be stained selectively in the case of TEM. Bates and coworkers[11,12] synthesized various series of polyolefin block copolymers in which one of the blocks was deuterated and these authors combined rheology and small angle neutron scattering (SANS) to show the morphological transitions of the microdomain induced by temperature and shear. However, it was necessary for the interpretation of the scattering data to assume a morphological model for the microdomain. Recently we have found that the morphology of DEP and APP blends in the melt state can be 'frozen' by quenching and at the same time the polyethylene block can crystallize within the microdomains[6]. We believe that this quenching technique enables us to observe the morphology in the melt state because crystals in the microdomain can provide enough contrast for both SAXS and TEM. In this paper, we study the morphology of micro- and macrophase separation of DEP and APP blends by employing this technique, and try to correlate the morphology and crystallization behaviour. In addition, SANS has been employed on the partially deuterated DEP and blends to observe the morphology in the melt state directly.

EXPERIMENTAL

Sample preparation

The samples of ethylene–propylene diblock copolymer (DEP), polyethylene (PE) and atactic polypropylene (APP) were prepared by hydrogenation of anionically synthesized poly(butadiene-*b*-2-methyl-1,3-pentadiene), polybutadiene and poly(2-methyl-1,3-pentadiene),

Table 1 Nomenclature and molecular characteristics

Sample	Nomenclature	M_w[a]	M_w/M_n[a]	Polyethylene content[b] (wt%)	Ethyl branch content[c] (mol%)	Density (g cm^{-3})
Ethylene–propylene diblock copolymer	DEP113	113,000	1.12	48	3.0	
				$f = 0.48$[d]		
	DEP99	99,100	1.07	50	3.0	
				$f = 0.50$[d]		
	d-DEP65[e]	64,800	1.07	53	3.0	
				$f = 0.52$[d]		
Atactic polypropylene	APP15	15,100	1.05	0	-	0.8500
	APP39	39,300	1.04	0	-	0.8510
	APP190	190,000	1.10	0	-	0.8515
Polyethylene	PE43	43,000	1.10	100	3.0	0.9145
High density polyethylene[f]	HDPE	53,000	3.0	-	-	0.9580

[a] Calculated from unhydrogenated precursors' results which were measured by gel permeation chromatography with low-angle laser light scattering. The calibration was done by standard polybutadiene samples
[b] From ^{13}C n.m.r.
[c] From ^{13}C n.m.r. and *FT*i.r. (in PE block for DEP)
[d] Symmetric factor defined as ethylene composition (vol%) in DEP calculated assuming the density of b-PE in the melt state to be 0.865 g cm^{-3}
[e] Used d-butadiene instead of butadiene
[f] Polyscience Inc., standard high density polyethylene (ASTM 1475)

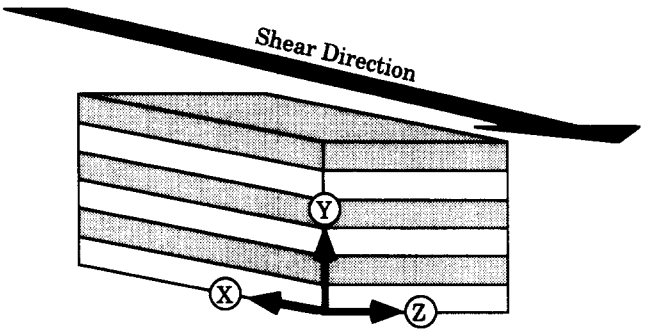

Figure 2 Definition of the coordinates used in this paper. Shear was always applied parallel to X, and the figure shows the proposed orientation for the lamellae as an example

respectively. For both the homopolybutadiene and the butadiene block, the microstructure was predominantly 1,4, with only 8% vinyl. The partially deuterated copolymer dDEP65, was made by using a perdeutero–butadiene as a monomer in the synthesis of the polydiene block polymer, followed by saturation with hydrogen. The details for the preparation of DEP, PE and APP have been described previously[5,13]. The molecular weight, branch content and other molecular characteristics for these samples are listed in *Table 1*, as well as the nomenclature used in this paper. Three series of blends; APP190 and DEP113, APP39 and DEP113, and finally APP15 and DEP113 and their deuterated analogues were investigated and the relative molecular weights ($M_{h\text{-APP}}/M_{b\text{-APP}}$) for the blends were 3.2, 0.67, and 0.26, respectively. The blending procedure and other sample preparation methods differed depending on the measurement technique used and therefore the details will be described in the following part.

In order to orient the microdomains, planar shear extension was applied to the melt state of DEP and to some blends with lower composition of APP in a specially designed flow cell[14]. The cell consisted of two lubricated parallel plates made of Teflon coated aluminium. In the cell the sample was compressed to between 1/4 and 1/6 of its original thickness in one direction, stretched in the second direction (extension direction), and held at a constant size in the third direction. The sample was maintained under pressure and annealed at 150°C for 2 h in vacuum. After that, the sample was immersed in liquid nitrogen together with the cell. These oriented samples served for TEM, scanning electron microscopy (SEM), SAXS and SANS. *Figure 2* defines the coordinates used in this paper. These coordinate axes will be referred to as the X view of TEM or (Z-Y) view in SAXS for instance. Here, the X view in TEM means an image observed for the section cut perpendicular to the X axis, and the X view in SAXS or SANS means a two-dimensional scattering pattern in the Y-Z plane when the X-ray or neutron beam was incident on a sample parallel to the X axis. Furthermore, the (Z-Y) scattering profile denotes sector averaged intensities along the Y axis in the Z view in SAXS, or SANS and Y-AZIM indicates the azimuthal average for the Y view.

Transmission electron microscopy

TEM observations were carried out at room temperature with a JEOL 100 CX electron microscope in the bright field mode with a potential of 100 kV. Ultra-thin sections of thin films were used as the specimens. Staining was not necessary for this system because the polyethylene crystals diffracted the electron beam hence providing diffraction contrast. The presence of characteristic electron beam diffraction rings from crystalline polyethylene was confirmed before taking micrographs.

Ultra-thin sections were cut from bulk blends which were made by solution mixing using hot toluene as a solvent. The DEP and APP solutions were prepared individually at a concentration of about 10 wt%, mixed together, filtered and poured onto a water surface the temperature of which was kept at 95°C, and then the solvent was evaporated. We believe that this procedure reduces inhomogeneities which might result from the crystallization of b-PE. DEP and the blends were annealed at 120–150°C for 5 days and quenched by immersion in liquid nitrogen. Some blends and DEP were subjected to shear extension as mentioned above. Ultra-thin sections of the samples were cut with a Reichert Ultracut microtome with a FC4 cryo temperature attachment using a glass knife. The temperature of the samples and the knife ranged between −100 and −50°C depending on the blend composition. Higher DEP compositions usually needed to be cut at lower temperature in order to obtain thin enough films for TEM observation.

Thin films of the blends were made by evaporating the solvent on a hot water surface. The blend solutions were prepared with concentrations of 0.5–0.1 wt% using a solvent mix of toluene and 1,2,4-trichlorobenzene. The solution was heated to above 80°C to dissolve the DEP completely, and a few drops of the solution were poured onto a hot water surface at around 90°C. The solvent was allowed to evaporate and after evaporation small pieces of the thin sample films were left on the water surface. These were picked up directly with TEM grids. The specimens on the TEM grids were annealed at 150°C for 3–5 days. After annealing, some specimens were quenched into liquid nitrogen and the others were cooled slowly over 2 days from 150°C to room temperature.

Scanning electron microscopy

Scanning electron microscopy was carried out for the blends of 10, 20, 30, 50 and 60 wt% of APP using a JEOL 35-CF SEM. The blends were made in the same way as the bulk blends. After annealing for 2 days at 120°C to allow the macrophases to develop to an approximately equilibrium state, the blends were quenched and immersed in toluene at room temperature for 1–12 h. Immersing the blends in toluene removed only the APP from the blends and formed holes in the surface as a result.

Small angle X-ray scattering

SAXS from the oriented samples was measured with the pinhole collimated 10 m camera at the National Center for Small Angle Research at Oak Ridge National Laboratory. The X-ray beam was generated by a rotating anode tube with a Ni filtered Cu Kα radiation source ($\lambda = 1.54$ Å) and collimated by a pinhole of 0.3 mm. The instrument was operated with a sample–detector distance of 5.176 m and a voltage of 40–44 kV for 1–4 h. Scattering patterns were measured by a two-dimensional position sensitive detector (20 × 20 cm) by

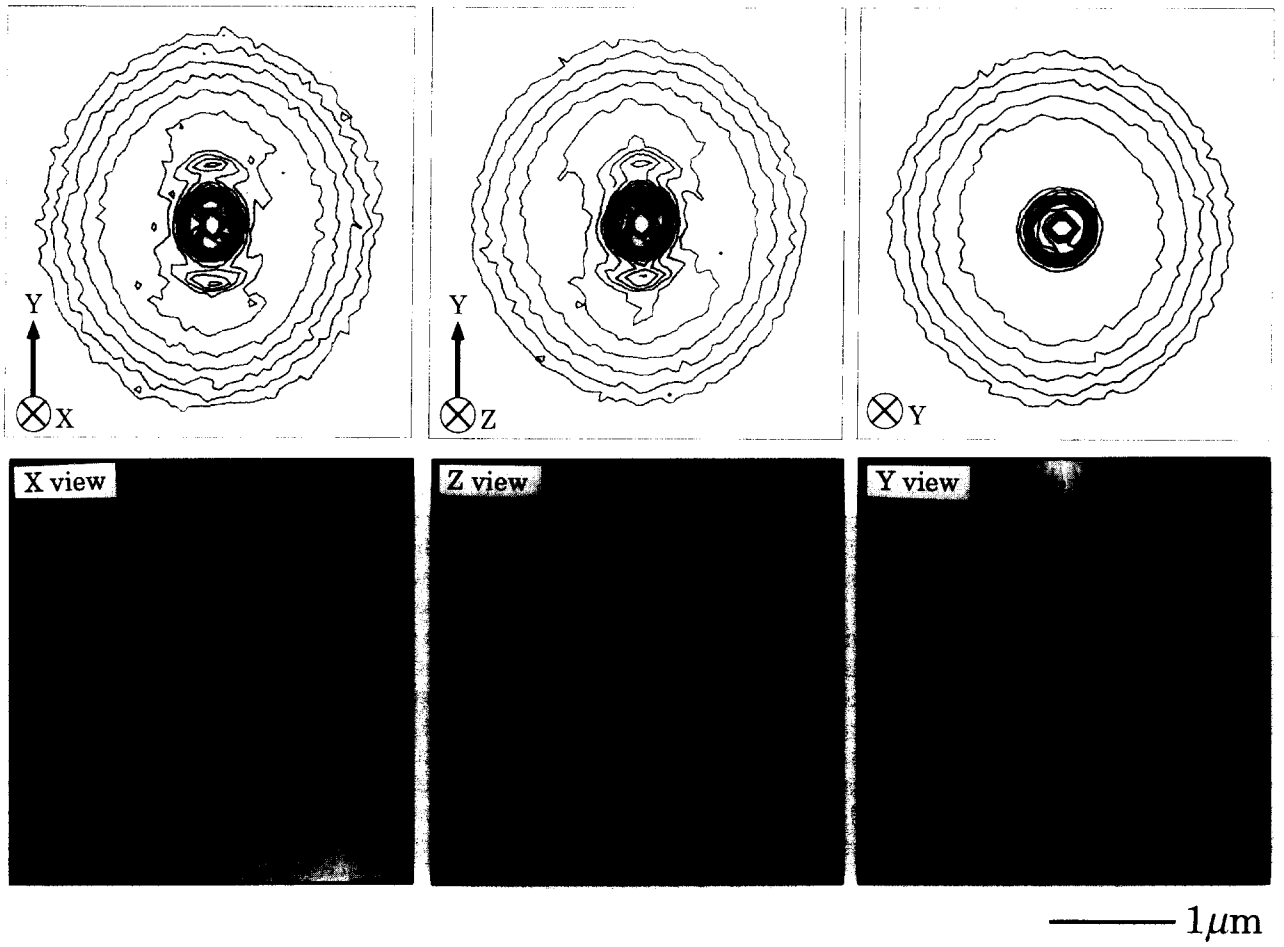

Figure 3 Two dimensional images obtained by TEM and SAXS for an oriented DEP113. The two figures on the left are the X views for SAXS (upper) and TEM (lower), the centre ones are the Z views and the right ones are the Y views

irradiating the X-ray beam parallel to the three directions, X, Y, and Z. The absolute intensities were obtained by calibration of sample thickness and with a polyethylene standard[15].

Small angle neutron scattering

The SANS experiments were carried out at the Cold Neutron Research Facility of the National Institute of Standards and Technology in Gaithersburg, MD. The wavelengths of the neutrons were 0.5 nm and sample–detector distances of 15 and 8 mm were used. Samples of both the pure diblocks and various blends were examined in orientations perpendicular and parallel to the lamellae, as described above.

Small angle light scattering

The small angle light scattering (SALS) patterns of the samples were taken with a laser light source of 632.8 nm under polarized conditions at room temperature. The blends were made in the same way as the bulk blends. Cooling conditions were found to change the scattering patterns significantly, so all samples were cooled slowly at an approximately constant rate over 2 days from 150°C to room temperature. The sizes of the spherulites were estimated from the SALS patterns using the Stein equation[16].

RESULTS AND DISCUSSION

Samples quenched from the melt state

Morphology of quenched DEP samples. *Figure 3* shows TEM and SAXS views for the X, Y, and Z direction of an oriented DEP113. In the TEM micrographs the dark area represents the b-PE rich phase because the b-PE crystallites diffract the electron beam and cause dark images in the bright field mode. The X and Z views in TEM show alternating lamellae of b-PE and b-APP extending parallel to X, which was the direction of the planar shear applied. The TEM image for the Y view can be explained by the presence of an undulation in the lamellar structure. SAXS patterns showed sharp meridian scattering with two or three maxima along the Y direction in the X and Z views, and a circular type diffuse scattering in the Y view, confirming the presence of highly oriented lamellae in the X-Z plane.

Figure 4 compares the angular dependence of SAXS intensities for different views of an oriented DEP113 as well as PE43 and an unoriented DEP113 sample. Two intense peaks were observed at $q = 0.08$ and $0.24\,nm^{-1}$ in the (Z-Y) and (X-Y) views. Both views were obtained by scattering the X-ray beam perpendicular to the direction of the lamella. Since q for the second most intense peak was three times larger than the first one, the two peaks can be assigned to the first and third order diffractions from the lamellar structure. The second order diffraction peak is either absent or is of very low intensity, perhaps being identified with the very weak peak at $q = 0.16\,nm^{-1}$. The small or absent second diffraction peak is due to cancellation by the weak intensity of the particle scattering function when the thickness of each lamellar domain is equal[10]. This is consistent with the

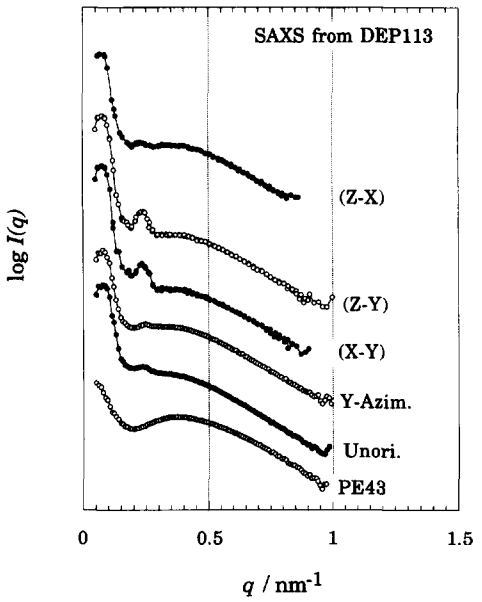

Figure 4 Angular dependence of the sector or azimuthal average X-ray intensities for DEP113. Unori. indicates the azimuthal average of scattering from the unoriented sample. The scattering intensities were corrected for the thickness of the samples and shifted by multiplying by an appropriate factor for convenience

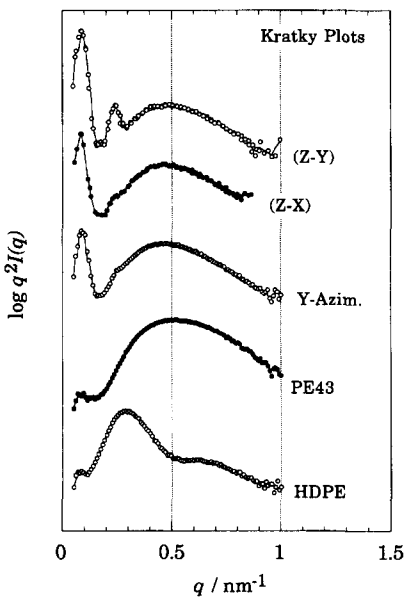

Figure 5 Comparison of the Kratky plots for (Z-Y), (Z-X) and Y views of an oriented DEP113, PE43 and HDPE

almost equal volume fraction of b-PE and b-APP in DEP113 (see *Table 1*). The scattering profiles for Y-Azim. and (Z-X) exhibit the first diffraction peak and a trace of the third one, although these are scattering from the parallel view to the lamellae. This feature suggests the presence of undulations of the domain structure or defects in the lamellae.

Figure 5 compares the Kratky plots for HDPE, PE43 and DEP113. The plots for PE43 and HDPE show broad maxima, which are typically observed for crystalline polymers and characterized as scattering from crystallines. Comparison of PE43 and HDPE show that PE43 has larger and more broadly distributed spacing in the crystallites than HDPE. This feature is consistent with the thermal data showing that PE43 has a lower degree of crystallinity and lower melting temperature than HDPE[5]. As mentioned in the previous papers[5,7] the lower crystallinity in PE43 and other related phenomena are caused by the fact that PE43 contains 3 mol% of ethyl branches. Scattering from the crystallites in DEP113 is weaker than from PE43 in line with the smaller scattering volume in the former. However, the maximum in DEP113 appears at almost the same position as in PE43. This indicates that the average spacing of the crystallites between DEP113 and PE43 is almost the same. In the case of the oriented samples, the scattering profiles of the (Z-X) and (Z-Y) views and also the scattering from an unoriented sample essentially agree with each other with respect to the peak shapes, intensities and positions. This suggests that the b-PE crystallites orient randomly within the lamellar domain.

Similar results were found for d-DEP65. Discussing first the results from the scattering in the X view, both SAXS and SANS gave a similar lamellar spacing at room temperature of about 52 nm for d-DEP65. The values of the spacing as well as those of other morphological variables can be found by fitting the data with the model of Agamalyan *et al.*[8] or that of Hashimoto *et al.*[9]. Three orders of peaks could be distinguished in the scattering patterns. The advantage of the ability to use SANS was that we could monitor changes in the spacings with heating. Up to 75°C (still below T_m), there was very little change. At 110°C, however, the peaks moved to higher angles, indicating a shrinkage of the spacing to around 47 nm. Moreover, five orders could be seen, indicating a more uniform distribution of the spacing. This can be seen in *Figure 6a*. Upon further heating the peaks moved to even higher angles, but fewer orders could be seen. Cooling to temperatures above crystallization showed reversibility of these results; after the samples recrystallized only the first peak remained, indicating that the orientation had been lost. This confirms the development of spherulites which has been seen in microscopy upon slow cooling.

The Y view scattering can be used to determine the interlamellar thickness[9]. Just as in the X view results discussed above, the most dramatic change occurred when the samples melted. At this point the thickness dropped from 6.0 to 1.8 nm. This is in line with the observation of more orders described above. There was also more structure in the scattering from this view than would have been expected if the lamellae were perfectly oriented, as can be seen in *Figure 6b*. This phenomenon may be due to differences in orientation in the lamellae or may arise from defects present in the lamellar structure. We are currently examining the question of this structure present in the Y view.

Figure 7 shows the molecular weight dependence of the SAXS profiles. With decreasing molecular weight from DEP113 to d-DEP65, the peak positions shift to larger q. Domain spacing (D) was evaluated in the normal way[10] and the results are summarized in *Table 2*.

When one block crystallizes within the microdomain, the equilibrium domain structure might be determined by the balance of the energy of chain folding and the conformational stretching free energy of the amorphous blocks[17,18]. Furthermore the crystallite must grow parallel to the domain boundary in order to remain within the domain. Whitmore and Noolandi[17], and DiMarzio *et al.*[18] independently calculated the molecular

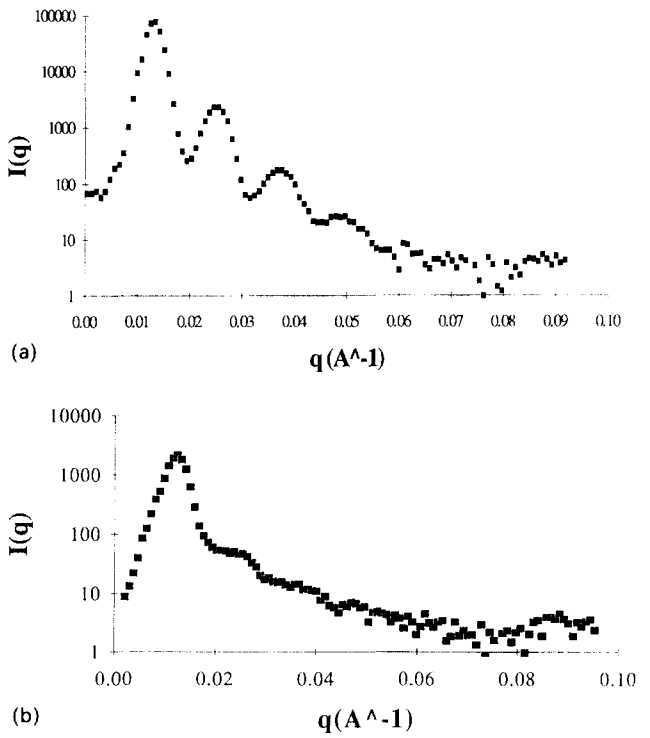

Figure 6 (a) Dependence of neutron scattering for d-DEP65 at 110°C. X view. (b) Dependence of neutron scattering for d-DEP65 at 110°C. Y view

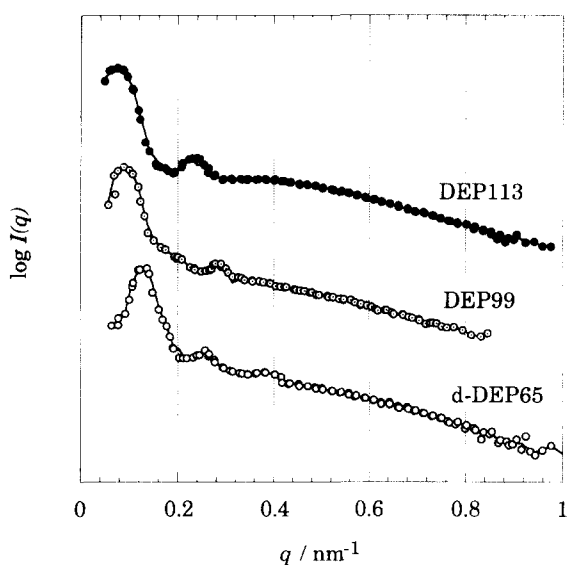

Figure 7 Molecular weight dependence of the SAXS profiles in the (Z-Y) view

weight dependence of the lamellar spacing based on this model. According to their theories

$$D \propto Z_t Z_a \alpha \qquad (1)$$

where D is the domain spacing of the lamellae, Z_t and Z_a are the number of the statistical segments for the total block and amorphous block, respectively, and a is a scaling factor which is given as $-1/3$ and $-5/12$ by DiMarzio *et al.* and Whitmore and Noolandi, respectively. Douzinas and Cohen[9] measured the lamellar domain spacing by SAXS for a series of hydrogenated 1,4-butadiene–1,2-butadiene diblock copolymers and compared their results with the theories. Their data agreed with Whitmore and Noolandi's calculation.

Table 2 Domain spacings obtained from SAXS

Sample	D (nm)
d-DEP65 (SANS)	52 ± 0.5
d-DEP65	48 ± 50
DEP99	68 ± 71
DEP113	78 ± 83
DEP113 + 5 wt% APP15	83 ± 92
DEP113 + 10 wt% APP15	90 ± 105

However, their WAXS data suggested that the crystallites aligned perpendicular to the domain interface. On the other hand, Rangarajan *et al.*[20] measured SAXS from block copolymers of hydrogenated 1,4-butadiene–1,4-isoprene diblock copolymers and proposed that the polyethylene crystallites preferentially aligned parallel to the lamellar microdomain. However, their data showed a stronger molecular weight dependence of the lamellar spacing than even Whitmore and Noolandi's calculation.

Our SAXS results show a random orientation of the crystallites in the b-PE microdomain and are inconsistent with the results of Douzinas *et al.* or Rangarajan *et al.* The work by these authors and our studies used the same crystalline block made through hydrogenation of poly(1,4-butadiene) and also the molecular weight range is similar, so it is necessary to comment on this discrepancy. One possible explanation is given by the difference in the sample preparation methods. We made our samples by quenching from the melt state, so the cooling rate may be too fast to reach equilibrium. Therefore applying the model for the equilibrium state may not be appropriate for our case. However, if cooled slowly over 2 days, which might be long enough to reach the equilibrium state, the lamellar microdomain structure was destroyed or heavily deformed as shown later, and also by SANS[6]. This fact indicates that for our case there is no equilibrium state with the b-PE crystallized within the lamellar domain. The other fact that should be noted is that the degree of crystallinity of b-PE is relatively small, ranging from 30–40%[5], so the crystallization may take place without direct influence from either the domain boundary or the other amorphous chain of b-APP. The model for the theories assumed complete crystallization of the crystalline block, and so the end of the folded chain has to be the junction point to the amorphous block. This restriction is the main cause for the alignment of the crystallite. However, in the case of hydrogenated poly(1,4-butadiene), the end of the folded chain can be located at any point within the b-PE domain due to the low crystallinity. This situation allows the crystallites to orient randomly.

Although our molecular weight range may not be wide enough to discuss the molecular weight dependence of the lamellar spacing, it is interesting to plot D/Z_t against Z_a for our case (*Figure 8a*). For three molecular weights, the values of D/M_w are almost independent of $M_{w\text{-}a}$. This feature is not consistent with either the theoretical predictions or the previous work by DiMarzio *et al.*[8] or Douzinas and Cohen[9]. *Figure 8b* plots D against M_w. The data points can be fitted by a straight line with the slope of 0.8. This value of the slope is close to the experimental results[21] for amorphous–amorphous diblock copolymers. This agreement confirms that we

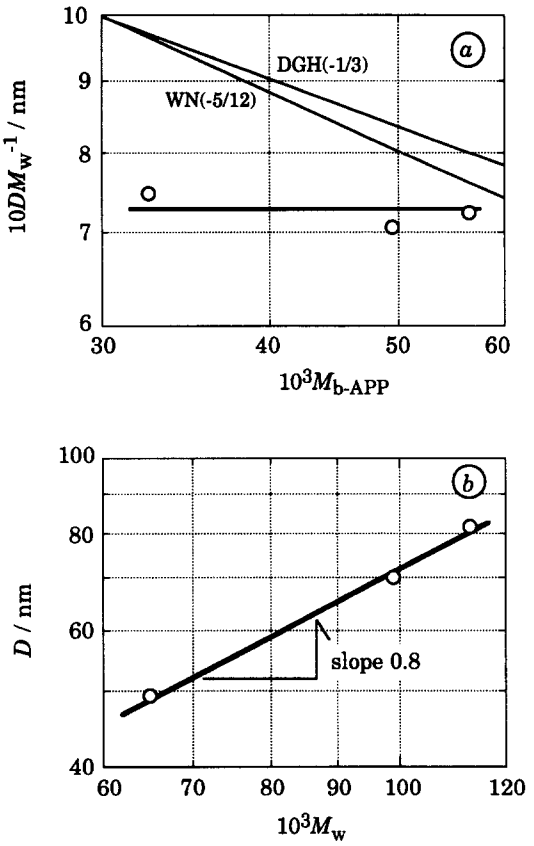

Figure 8 Scaling plots for the molecular weight dependence of the lamellar domain spacing. In (*a*) WN and DGH indicate theoretically predicted slopes by Whitmore and Noolandi[17], and DiMarzio *et al.*[18], respectively

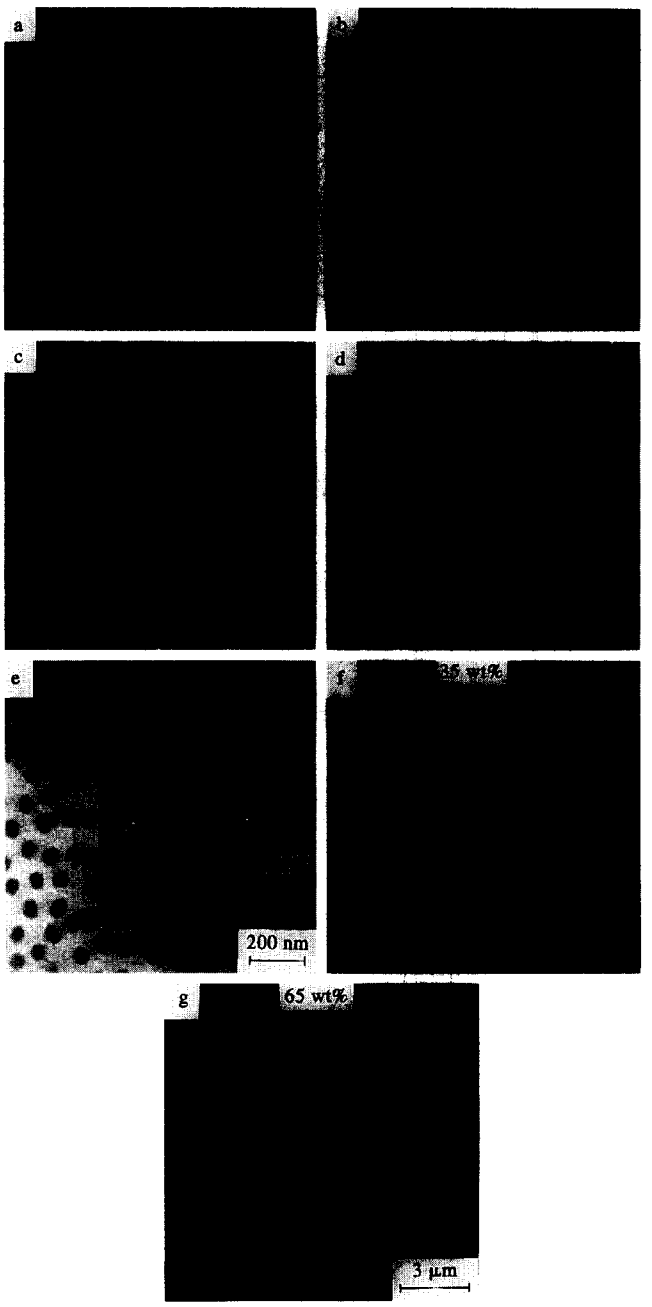

Figure 9 TEM bright field micrographs for the blends of DEP113 and APP15. The bright area consists of a mixture of b-APP and h-APP and also some micrographs show the b-PE crystallites as black specks in the dark area. (a) 15%, Z-view, lamellae, (b) 25%, a microtomed section from an unoriented sample, (c) (f) 35%, a cast thin film, CNC, (d) (g) 65%, a cast thin film, isolated cylinders, (e) 80%, a microtomed section from the unoriented sample, randomly oriented micelles. *Figure 14* also shows isolated cylinders observed from 50 wt% blend

could 'freeze' the domain structure in the melt state by the quenching technique.

Morphological transitions in the blends of APP15 and DEP. For the blends of DEP113 and APP15, *Figure 9* shows TEM micrographs and *Figures 10* and *11* present two dimensional images and (Z-Y) views of SAXS, respectively. As determined by both experiments, there are three composition regimes giving different types of microdomain structures in the blends. The first is up to 10 wt%, the second is between 20% and 40%, and the third is above 50 wt%. Here it should be mentioned again that these microdomain structures are considered to be the morphologies in the melt state because the samples were 'frozen' by quenching from 150°C by immersion in liquid nitrogen.

As shown in *Figure 11*, up to 10 wt% of APP15, (Z-Y) views of SAXS showed two peaks, the same features as in DEP113, indicating that the microdomain still maintains the lamellar structure. *Table 2* summarizes the lamellar spacing obtained from SAXS and the comparison of three compositions (0, 5 and 10 wt% of APP15) shows the increment of the lamellar spacing with increasing APP. However, as shown in TEM and the 2D image for the 10% blend, blending caused the lamellar structure to become less aligned and more undulating.

From the SAXS data in *Figures 10* and *11*, it seems that a structural transition occurs between 10 and 20 wt%. Above 20 wt% the second peak disappears and the first main peak shifts under the beam stop. For TEM, in the composition range of 20–40 wt%, in fact, it was difficult to obtain clear images by microtoming the quenched blends. As shown in *Figure 9b* for instance, the TEM micrograph for the 35 wt% blend is not easy to interpret, but it seems that the b-PE crystalline rich phase is entangled with itself in a similar manner to homo PE. On the other hand, ultra-thin films of the blends exhibit distinct changes from the lamellar microstructure. An example is shown in *Figure 9c*. The cylindrical b-PE crystalline phases are linked to each other to make a network like structure. The planar phases in the micrograph can be understood to consist of mixtures of b-APP and h-APP and also the b-PE crystallites can be

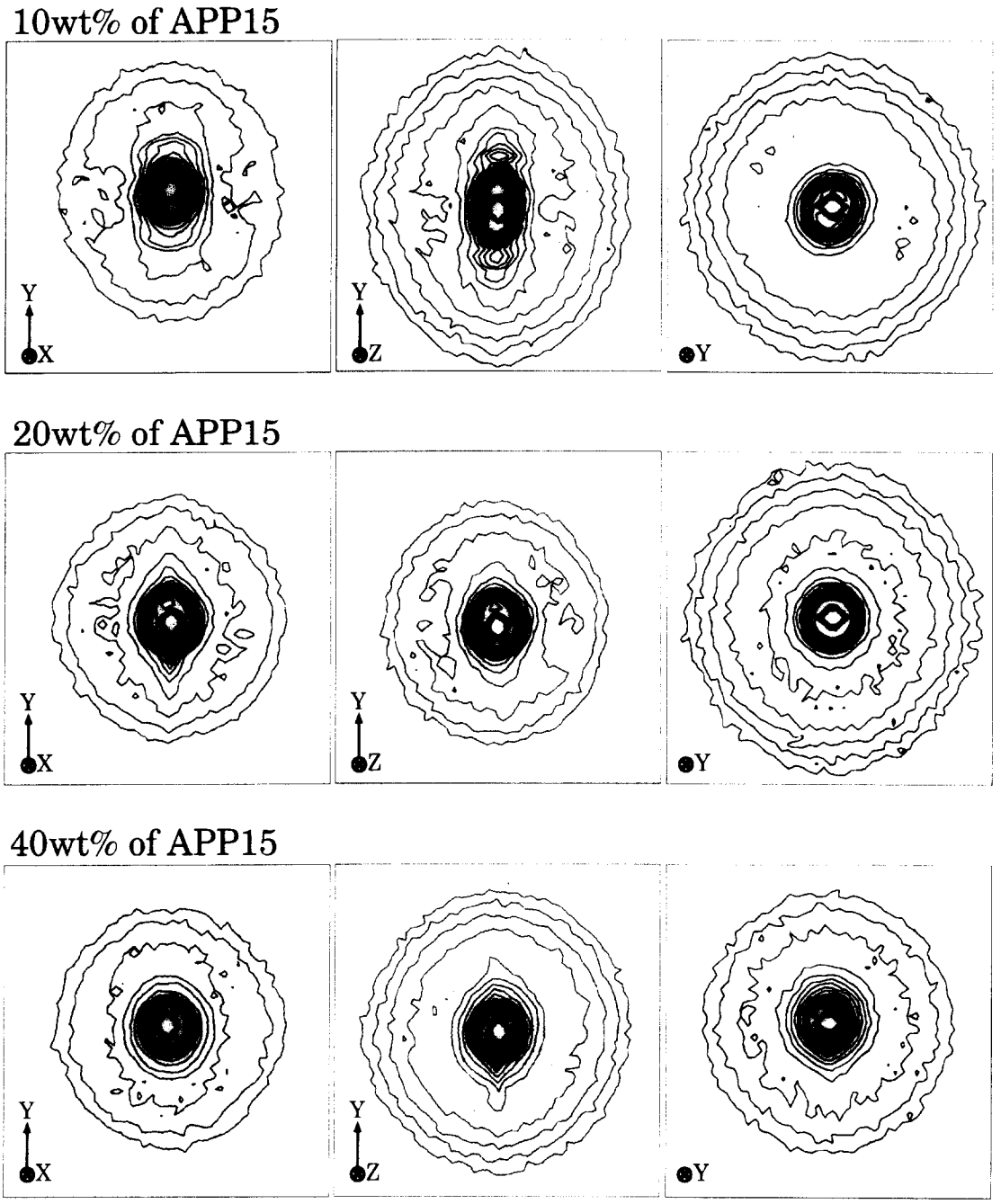

Figure 10 Changes in the SAXS two dimensional patterns for the oriented samples upon blending DEP113 and APP15

observed as black specks in the dark phase. Since the thin film images were presumably obtained by two-dimensionally extending the bulk, both the b-PE domain and the APP domain are continuous in the bulk[22]. Therefore this structure can be classified as a bicontinuous structure.

SANS was also used to examine the blends of APP15 and dDEP65. Addition of APP15 to dDEP65 increased the value of the lamellar spacing only slightly, in line with the amount added. This indicates that it was to be found totally within the APP lamellae from the block polymer, without any macrophase separation. As with the neat dDEP65, the blend spacing became sharper upon melting and expanded a small amount as the temperature increased. This order was essentially lost upon cooling, a sign that spherulites were formed in the blends as well.

Winey *et al.*[2] observed a hexagonally packed cylindrical structure for the polystyrene/polybutadiene or polystyrene/polyisoprene system at the same composition range that we observed the bicontinuous structure. If our system had formed the same hexagonal packed cylindrical structure, we should have observed six intensity maxima aligned with an azimuthal angle of 60° in the X view in SAXS. The fact is that the X view did not show such a pattern, although some structural alignment exists in the Y direction. We did observe a cylindrical structure in TEM, but it was not hexagonally packed. At present the reason for this is not clear. One possible explanation is that although the molecular weights of Winey's samples are about 100×10^3, which is the same molecular weight range as ours, in terms of the Kuhn segment number or number of entanglements[23], the statistical length of our polymer chains is almost ten times longer than that of the styrene/butadiene or

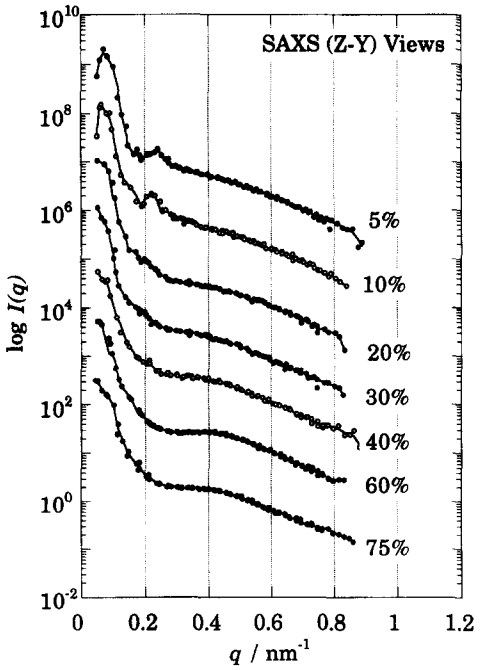

Figure 11 Composition dependence of SAXS (Z-Y) view for the blends of DEP113 and APP15. The values in the figure indicate weight percent of APP15 in the blends

styrene/isoprene system. Therefore our blends may be kinetically trapped before reaching their thermodynamic equilibrium state which might be a hexagonally packed cylindrical structure.

When the composition of APP15 increased from 40 to 50 wt% in the blends, a significant change occurred in the TEM micrographs for the thin films. At 40 wt%, the b-PE phase constituted a network structure (*Figure 9c*). Once the composition exceeded 59 wt%, the cylinders became discontinuous and isolated from each other. *Figure 9d* shows an example of these discrete or isolated cylindrical structures. Furthermore at 75 wt% APP, randomly oriented spheres were observed as shown in *Figure 9e*. According to Winey *et al.*[2], these isolated domains are classified as disordered micelles.

Macrophase separation. The presence of macrophase separation was detected by SEM observation of the surface of the samples which had been immersed in toluene. Examples of SEM micrographs are shown in *Figure 12* for the blends with 50 wt% of APP. The APP15 blends show a smooth surface indicating the absence of macrophase separation. On the other hand, APP39 and APP190 blends show holes and surface roughness which arise presumably from the toluene extraction of an APP rich macrophase. The results of the SEM study are depicted in *Figure 13*.

Surface observation by SEM may not be the best way to determine exactly the boundary of macrophase separation because errors can be caused by the sample preparation and the subjective judgement. In fact, for the blend with more than 60 wt% of APP, the extraction was not successful sometimes due to swelling or dispersion of the samples into the solvent. Therefore, the boundary for macrophase separation in *Figure 13* has some ambiguity, especially for the higher APP compositions, and its exact determination requires scattering techniques. When we attempted to make oriented samples by applying planar

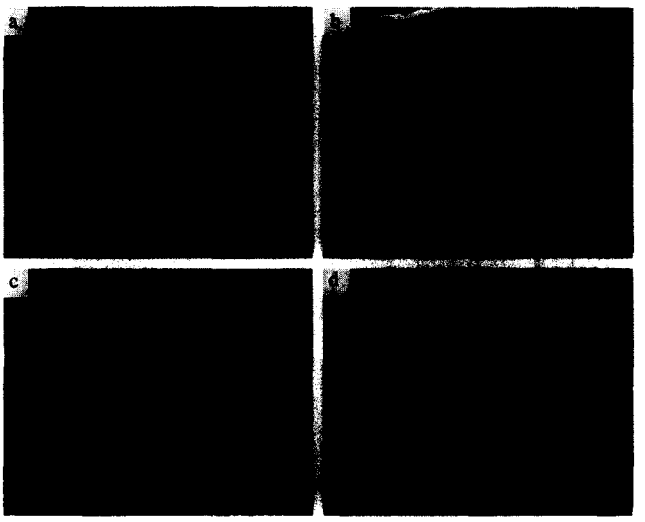

Figure 12 Examples of SEM observations for the surface of the 50 wt% blends. (a) APP190 blend before immersion in toluene; (b) APP190 blend; (c) APP39 blend; (d) APP15 blend

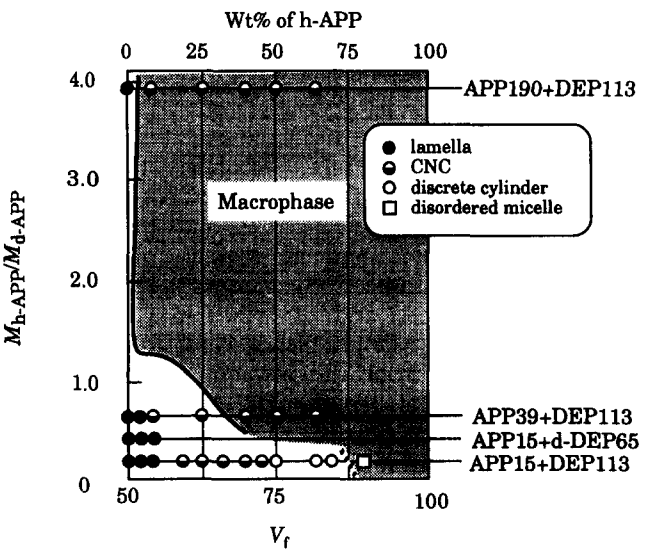

Figure 13 A morphological diagram for the blends constructed from TEM, SEM, SANS and SAXS experiments

shear extension to some blends of APP190 or APP39, APP was squeezed out from the blends and so we could not make homogeneously mixed blends for TEM or SAXS. That phenomenon confirms that macrophase separation occurred.

Microdomain structures in the blends with APP190 or APP39 and DEP113. For APP39 and APP190 blends, TEM micrographs for the thin films always showed network structures. *Figure 13* includes these results and *Figure 14* shows the examples. For both APP190 and APP39 blends, the micrographs shown are for the composition of 50 wt%. At the same composition, the APP15 blend showed a discrete cylindrical structure (*Figure 9d*). Although both patterns in *Figure 14* can be classified as network structures, there is some difference between these patterns. In APP190 blends spheres are observed, the size of the network is smaller and more deformed than in APP39 blends, and b-PE cylinders seem to show more tendency to crowd together than in APP39 blends. Tanaka *et al.*[24] simulated pattern formation of the macrophase domains during phase separation

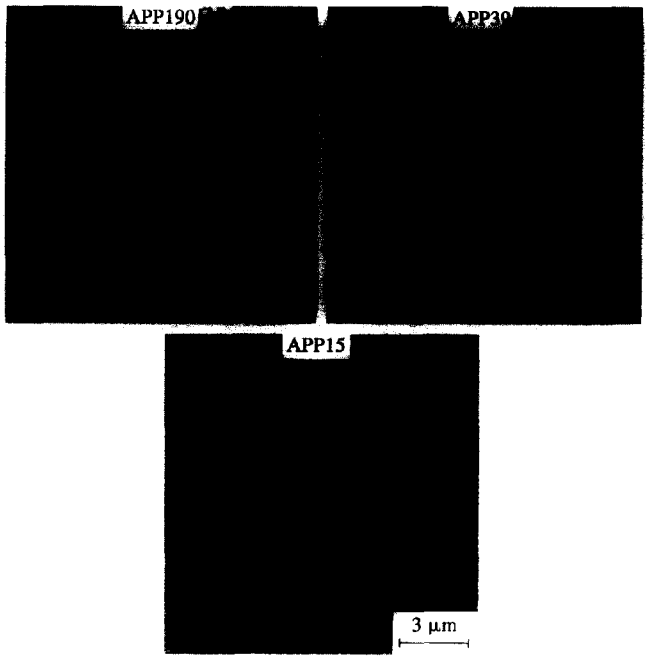

Figure 14 CNC observed for the blends with 50 wt% of APP39 and APP190. At the same composition, the APP15 blend shows an isolated cylinder morphology

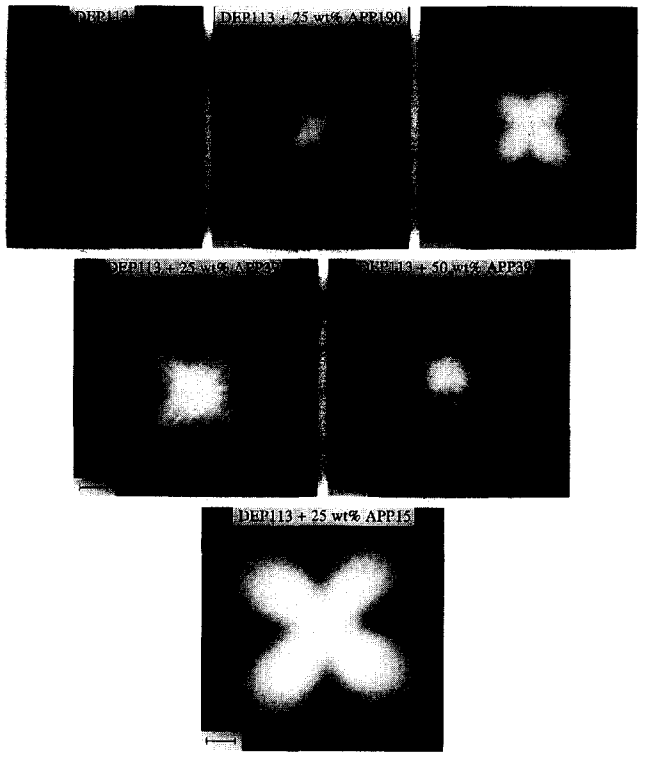

Figure 15 Comparison of the SALS patterns for the blends. The white bars correspond to a scattering angle of 1.8°

by using Boloni's diagram. According to them the patterns can be classified in three types: cluster, regular, and random, and each type corresponds to the case of repulsion, attraction, and no special force between different domains, respectively. Comparing TEM micrographs in *Figures 9d* and *14* with Tanaka's diagram, APP15 blends and APP190 blends show similar features to those arising from the attraction and repulsion patterns, respectively. Although additional TEM is needed, it might be possible to evaluate some driving force for phase separation by using image analysis of TEM micrographs.

Morphological diagram and crystallization kinetics

Based on SAXS, SANS, TEM, and SEM, a morphological diagram for the blends (*Figure 13*) has been constructed as a function of the relative molecular weight and the overall APP volume fraction in the blends. The diagram, consistent with SANS results, represents morphological changes in the melt state of the blends, that is in the amorphous state. Comparing with Winey *et al.*'s diagram[2] for the blends of amorphous diblock copolymers and amorphous homopolymers, our morphological diagram is consistent with their results in the major features. Therefore our phase behaviour can be rationalized in terms of the same principle as these authors used. According to them and some theoretical work[25], the ratio of molecular weight between the block and the homopolymer, for our case, APP and polypropylene block in DEP ($M_{h\text{-APP}}/M_{b\text{-APP}}$) plays a critical role. In the case of $M_{h\text{-APP}}/M_{b\text{-APP}} > 1$, macrophase separation takes place in almost the entire composition range. This is because the size of the APP chain is too large to merge into the microdomain of the APP block. On the other hand, in the case of $M_{h\text{-APP}}/M_{b\text{-APP}} < 1$, macrophase separation is suppressed and blending causes a morphological transition of the microdomain. The reason for this is that the lower molecular weight homopolymer can enter into the A rich phase in the microdomain and thus change the volume fraction of the domain and the interfacial free energy, and so induce the morphological transition.

Table 3 Molecular weight and composition dependence of the radius of spherulites for APP and DEP113 Blends

Sample	Spherulite radius (μm)
DEP113	70 ± 5
DEP113 + 25% APP190	10 ± 1
DEP113 + 50% APP190	8 ± 2
DEP113 + 25% APP39	8 ± 2
DEP113 + 50% APP39	10 ± 3
DEP113 + 25% APP15	5 ± 2
DEP113 + 50% APP15	no pattern

The diagram in *Figure 13* clearly corresponds to the crystallization behaviour described in our previous paper[5] (see *Figure 1* for example). The region for lamellar and bicontinuous structures in the diagram corresponds to that for Peak I and the micelle region always gives Peak II. The Avrami exponent for APP15 blends changes from 2 to 1.5 at the composition of 50 wt%, which is the same composition for the transition from the bicontinuous to the micelle structure by TEM. These agreements provide evidence for the hypothesis that different microdomain structures are responsible for the different crystallization behaviour, Peaks I and II and the different Avrami exponents.

Spherulite formation by slow cooling from the melt state

In *Figure 15* the SALS patterns are compared for DEP113 and its blends with APP190, APP39 and APP15 for the composition of 25 and 50 wt%, and the radii of the spherulites are summarized in *Table 3*. Since the 50 wt% APP15 blend did not show any four-leaf clover pattern, the result is not presented here. The size of the

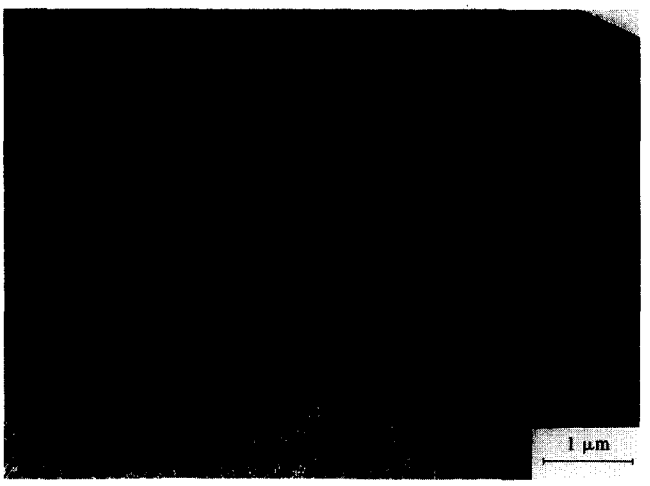

Figure 16 Sheaf-like structures in a thin film blend observed by TEM. The composition is 25 wt% of APP15 in the DEP113 blend and the film was cooled slowly from 150°C during 2 days

spherulites in DEP113 is relatively large compared with the blends and with increasing APP content or decreasing APP molecular weight, the size becomes smaller and the pattern also becomes smeared. In the melt state, b-PE forms a lamellar structure for DEP113 and then continuous cylindrical structures for the blends with 25 and 50 wt% of APP190 and APP39, and 25 wt% of APP15. When cooled from these morphologies, spherulites could form much more easily from lamellae than from cylinders. That structural difference rationalizes the differences in the sizes of the spherulites. Furthermore it must be more difficult or maybe impossible for spherulites to form from isolated cylinders because crystallites cannot grow beyond the phase boundary. This is the reason for the absence of scattering patterns for the 50 wt% APP15 blend. Crystallization is a more favourable thermodynamic transition than phase separation, so once it occurs the morphology in the melt state must be affected. *Figure 16* shows an example for the TEM micrographs for thin film blends which were cooled slowly from the melt state. A sheaf-like structure is present which is typically observed for the intermediate stage in the formation of spherulites. *Figure 9c* shows a TEM micrograph of the same thin film blend. Comparing these two results reveals that crystallization completely destroys the microdomain structures in the melt state when cooling is slow enough to achieve equilibrium.

CONCLUSION

SANS, SAXS, TEM and SEM reveal that DEP forms a lamellar microdomain structure and blending DEP with APP induces morphological changes in the microdomains. In the case of APP15 blends blending changes the morphology from a lamellar to a bicontinuous cylindrical and then a discrete cylindrical and finally to a spherical microstructure. On the other hand, APP39 and 190 blends undergo macrophase separation and only a transition from lamellae to bicontinuous cylinders occurs. These morphological transitions in the melt state are correlated with the crystallization kinetics of the blends. Slow cooling results in complete destruction of the microstructure and allows spherulites to develop.

ACKNOWLEDGEMENTS

We thank Mr E. Habeeb and Mr R. Krishnamoorti for their assistance with hydrogenation. We also acknowledge Prof. M. Muthukumar, Prof. S. Kumar, Dr L. J. Fetters, and Dr T. P. Russell for helpful discussions. K.S. extends appreciation to Kanebo Ltd. for providing him the opportunity to work on this project. Acknowledgment is made to the UMASS Material Research Laboratory, funded by the National Foundation for support through the use of the central facilities.

REFERENCES

1 Hashimoto, T., Tanaka, H. and Hasegawa, H. in 'Molecular Conformation and Dynamics of Macromolecules in Condensed System' (Ed. M. Nagasawa), Elsevier Science, Oxford, 1988, p. 257
2 Winey, K. I., Thomas, E. L. and Fetters, L. J. *Macromolecules* 1992, **25**, 2645
3 Winey, K. I., Thomas, E. L. and Fetters, L. J. *Macromolecules* 1992, **25**, 422
4 Thomas, E. L., Anderson, D. M., Henkee, C. S. and Hoffman, D. *Nature* 1988, **334**, 598
5 Sakurai, K., MacKnight, W. J., Lohse, D. J., Schulz, D. N. and Sissano, J. A. *Macromolecules* 1994, **27**, 4941
6 Sakurai, K., MacKnight, W. J., Lohse, D. J., Schulz, D. N., Sissano, J. A. and Agamalyan, M. *Am. Chem. Soc. Div. Polym. Mater. Sci. Eng. Prepr.* 1993, 69
7 Sakurai, K., MacKnight, W. J., Lohse, D. J., Schulz, D. N. and Sissano, J. A. *Macromolecules* 1993, **26**, 3236
8 Agamalyan, M., Evmenko, G. A., Vilesou, A. D., Frenkel, S. Y., Zponik, V. N., Vinogradov, V. and Milemevskaya, E. Y. *Polymer* 1992, **22**, 2542
9 Hashimoto, T., Toda, A., Ito, H. and Kawai, H. *Macromolecules* 1977, **10**, 377
10 Hashimoto, T., Tanaka, H. and Hasegawa, H. *Macromolecules* 1990, **23**, 4378
11 Hamley, I. W., Koppi, K. A., Rosedale, J. H., Bates, F. S., Almdal, J. and Mortensen, K. *Macromolecules* 1993, **26**, 5959
12 Almdal, K., Koppi, K. A., Bates, F. S. and Mortensen, K. *Macromolecules* 1992, **25**, 1743
13 Xu, Z., Mays, J. W., Chen, X., Hadjichristidis, N., Schilling, F., Bair, H. E., Pearson, D. S. and Fetters, L. J. *Macromolecules* 1985, **18**, 2560
14 Scott, D. B., Waddon, A. J., Lin, Y., Karasz, F. E. and Winter, H. H. *Macromolecules* 1992, **25**, 4175
15 Russell, T. P., Lin, J. S., Spooner, S. and Wignall, G. D. *J. Appl. Cryst.* 1988, **21**, 629
16 Stein, R. S. in 'Polymer Blends' (Ed. D. R. Paul and S. Newman), Vol. 1, Academic Press Inc., New York, 1978, p. 393
17 Whitmore, M. D. and Noolandi, J. *Macromolecules* 1988, **21**, 1482
18 DiMarzio, E. A., Guttman, C. M. and Hoffman, J. D. *Macromolecules* 1980, **13**, 1994
19 Douzinas, K. C. and Cohen, R. E. *Macromolecules* 1992, **25**, 5030
20 Rangarajan, P., Register, A. R. and Fetters, L. J. *Macromolecules* 1993, **26**, 4640
21 Hashimoto, T., Shibayama, M. and Kawai, H. *Macromolecules* 1980, **13**, 1237
22 In some block copolymers, morphology in their films can differ from that in bulk due to surface tension or difference in affinity to the air between the segments. This thin film effect is usually observed near the order–disorder transition. For strongly segregated blends the thin film morphology is the same as that in the bulk. In our case rheological measurements have confirmed that the phases were strongly segregated in DEP113
23 Ferry, J. D. 'Viscoelastic Properties of Polymers', 3rd Edn, Wiley, 1980, p. 374
24 Tanaka, H., Hayashi, T. and Nishi, T. *J. Appl. Phys.* 1989, **65**, 4480
25 Whitmore, M. D. and Noolandi, J. *Macromolecules* 1984, **17**, 2847